ACS APPLIED MATERIALS & INTERFACES

Research Article

www.acsami.org

Chemical Self-Doping of Organic Nanoribbons for High Conductivity and Potential Application as Chemiresistive Sensor

Na Wu,[†] Chen Wang,[†] Benjamin R. Bunes,[†,‡] Yaqiong Zhang,[†] Paul M. Slattum,[‡] Xiaomei Yang,[†] and Ling Zang*[,†]

[†]Nano Institute of Utah and Department of Materials Science and Engineering, University of Utah, 36 South Wasatch Drive, Salt Lake City, Utah 84112, United States

[‡]Vaporsens, Inc., 36 South Wasatch Drive, Salt Lake City, Utah 84112, United States

Supporting Information

ABSTRACT: Intrinsically low electrical conductivity of organic semiconductors hinders their further development into practical electronic devices. Herein, we report on an efficient chemical self-doping to increase the conductivity through one-dimensional stacking arrangement of electron donor−acceptor (D−A) molecules. The D−A molecule employed was a 1-methylpiperidine-substituted perylene tetracarboxylic diimide (MP-PTCDI), of which the methylpiperidine moiety is a strong electron donor, and can form a charge transfer complex with PTCDI (acting as the acceptor), generating anionic radical of PTCDI as evidenced in molecular solutions. Upon self-assembling into nanoribbons through columnar $\pi-\pi$ stacking, the intermolecular charge transfer interaction between methylpiperidine and PTCDI would be enhanced, and the electrons generated are delocalized along the $\pi-\pi$ stacking of PTCDIs, leading to enhancement in conductivity. The conductive fiber materials thus produced can potentially be used as chemiresistive sensor for vapor detection of electron deficient chemicals such as hydrogen peroxide, taking advantage of the large surface area of nanofibers. As a major component of improvised explosives, hydrogen peroxide remains a critical signature chemical for public safety screening and monitoring.

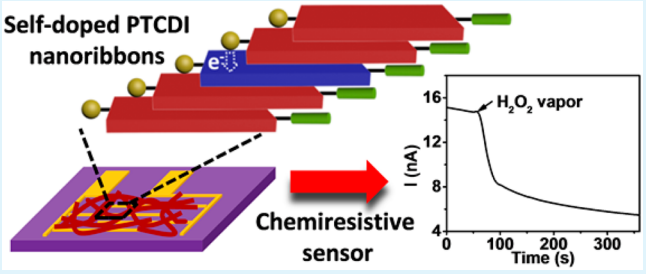

KEYWORDS: *organic semiconductor, electrical conductivity, nanoribbon, self-doping, chemiresistive sensor*

1. INTRODUCTION

Organic semiconductors are an alternative to conventional inorganic semiconductors and offer advantages such as mechanical flexibility and ease of solution processing. They have been applied in varying electronic devices, including organic field-effect transistors (OFETs),[1] organic light-emitting diodes (OLEDs),[2] photovoltaics,[3] photodetectors,[4] and sensors.[5,6] Unfortunately, their intrinsically low electrical conductivity,[7] due to properties such as the closed-shell electronic structures of the individual organic molecules and weak intermolecular interactions, hinders further development and more widespread applications. Studies have shown that electrical doping of organic semiconductors is an effective strategy to overcome this limitation,[8] enhancing conductivity by many orders of magnitude. Doping requires matched energy levels (redox potentials) between the host molecules and dopants.[8] Hence, the number of dopants is limited. Common dopants are small molecules such as O_2,[9] Br_2, I_2[10] and larger molecules such as F4-TCNQ (perfluorinated tetracyanoquinodimethane),[11] and pyronin B.[12] Nevertheless, all of these are interstitial dopants which are mobile in the host materials,[8] so the electrical properties of the doped organic semiconductors may change in time as the dopants diffuse. Therefore, exploration of a new type of dopant is important for achieving high-quality organic semiconductor materials.

Substitutional n-type doping was previously achieved by introducing a zwitterionic dopant to the perylene tetracarboxylic diimide (PTCDI) molecules.[13−15] The dopant was a reduced species (anionic radical) of the host molecule, so they did not significantly alter the crystal structure and were fixed in the semiconductor lattice. The conductivity was dependent on the concentration of dopant and showed large enhancement even with small amount of dopants. Anionic radicals of PTCDI molecules can also be generated by interacting with reducing agent like hydrazine.[16] After exposure to hydrazine vapor, the nanobelts self-assembled from PTCDIs increased conductivity because of the formation of PTCDI anionic radicals, which provide electrons as the major charge carrier rapidly migrating along the long axis of nanobelt through $\pi-\pi$ delocalization. With the similar process and mechanism, OFETs based on hydrazine doped PTCDI molecules were fabricated to achieve lower operating voltages and higher conductivity.[17]

Received: March 14, 2016
Accepted: May 2, 2016
Published: May 2, 2016

DOI: 10.1021/acsami.6b03151
ACS Appl. Mater. Interfaces 2016, 8, 12360−12368

Inspired by these works, we designed PTCDI molecules substituted with 1-methylpiperidine (MP) to construct self-doped semiconductor through one-dimensional (1D) self-assembly of the molecules into nanoribbons structure. The methylpiperidine moiety on one molecule, a strong electron donor (D), interacted with PTCDI on the other molecule (acting as the electron acceptor, A), generating anionic radicals of PTCDI. The resultant radicals functioned as the n-type dopants located in the lattice of the PTCDI semiconductors.[13−15] The similar side-group induced self-doping has also been widely exploited in conducting polymer materials (e.g., polyaniline).[18,19] The nanoribbon structure, dominated by the $\pi-\pi$ stacking between the PTCDI planes, provides an efficient pathway for long-range charge transport.[20] The nanoribbons reported in this study exhibited 4 orders of magnitude higher current compared to the 1D nanomaterials assembled from other PTCDI molecules under the same test conditions.[21]

With high conductivity, the n-type PTCDI nanoribbons can potentially be developed as a chemiresistive sensor for detection of electron deficient chemicals with a high signal-to-noise ratio, providing more reliable output signal and lower limit of detection. As evidenced in this study, the PTCDI nanoribbons demonstrate sensitive chemiresistive response to the hydrogen peroxide (H_2O_2) vapor, enabling potential application in detection of improvised explosives, such as triacetone triperoxide (TATP), diacetone diperoxide (DADP), hexamethylene triperoxide diamine (HMTD), and simple liquid mixtures of concentrated hydrogen peroxide and fuels (e.g., alcohols, acetone).[22] H_2O_2 is commonly used as the chemical marker of these peroxide explosives. Current techniques for detecting H_2O_2 are fluorometric,[22−24] colorimetric,[25] and electrochemical methods,[26] but most of them are limited to detection in the liquid phase. It is still challenging to detect H_2O_2 vapor at trace level. The chemiresistive sensing technique has the advantages of trace vapor detection and enables fabricating a portable, low-power, and simple sensor device.[27,28]

2. EXPERIMENTAL SECTION

2.1. Synthesis of *N*-Dodecyl-*N*′-[(1-methylpiperidine-4-yl)-methyl]-perylene-3,4,9,10-tetracarboxylic Diimide (MP-PTCDI). The precursor compound, *N*-dodecyl-perylene-3,4,9,10-tetracarboxylic monoimide monoanhydride (Compound 1, Figure S1), was synthesized using a previous method.[21] Subsequently, Compound 1 (100 mg), (1-methyl-4-piperidinyl)methanamine (Sigma-Aldrich, 71.3 mg), zinc acetate (Sigma-Aldrich, ACS reagent, 98%, 3.0 mg) and imidazole (Sigma-Aldrich, ACS reagent, > 99%, 1.5 g) were combined and heated to 150 °C for 8 h. After cooling to room temperature, the reaction mixture was dispersed in 10% HCl (Fisher Chemical, 36.5−38.0%, w/w) solution to solubilize the imidazole, the insoluble product was collected by filtration and washed with water and methanol. The crude product was converted to the free base by dissolving in chloroform and washing with 10% NaOH (Sigma-Aldrich, ACS reagent, > 97.0%) solution. The organic layer was washed with water and dried over anhydrous Na_2SO_4 (Sigma-Aldrich, ACS reagent, > 99%). The reaction mixture was then purified by silica gel chromatography using 6.0% ethanol in chloroform as the eluent followed by recrystallization from chloroform/ethanol to give final product (54.7 mg, 46%). ^{1}H NMR (500 MHz, $CDCl_3$, TMS, ppm): δ = 8.65 (d, J = 8.0 Hz, 4H; perylene H), 8.57 (d, J = 8.0 Hz, 4H; perylene H), 4.21−4.14 (m, 4H; $(CO)_2NCH_2$), 2.87 (m, 2H; CHH*N (CH_3)CHH*), 2.26 (s, 3H; NCH_3), 1.96−1.88 (m, 2H; CH*HN (CH_3)CH*H), 1.79−1.71 (m, 4H; $(CH_2*)_2CHCH_2N$), 1.34−1.22 (m, 21H,10CH_2, CH), 0.87 (t, J = 6.84 Hz, 3H; CH_3); ^{13}C NMR (125 MHz, $CDCl_3$, TMS, ppm): δ = 173.26, 163.88, 163.53, 137.05, 134.87, 134.70, 131.72, 131.56, 129.62, 129.54, 126.62, 123.60, 123.39, 123.32, 123.26, 116.49, 115.30, 55.65, 46.52, 40.95, 32.13, 30.46, 29.91, 29.84, 29.77, 29.60, 29.56, 28.34, 27.39, 22.89, 14.31. MALDI-TOF-MS: $[M + H^+]/z$ = 670.35.

2.2. Fabrication of Nanoribbons. Self-assembly of the MP-PTCDI molecules was performed through a solvent exchange process from a "good" solvent to a "bad" solvent, where the molecules have limited solubility in the "bad" solvent and thus self-assemble into 1D nanostructures via molecular stacking.[21] In this study, we used a solution injection method to conduct the self-assembly in ethanol. Typically, 0.4 mL of MP-PTCDI solution (1.5 mmol/L) in chloroform was injected rapidly into a larger volume of ethanol (4 mL) and placed in the dark for 5 h. The nanoribbons were then transferred to substrates for further characterization and electrical measurements. Synthesis of MA-PTCDI and MO-PTCDI, and self-assembly into nanoribbons were performed according to the previously reported methods.[21] Synthesis of CH-PTCDI molecules and self-assembly into nanobelts were based on the previously reported methods.[29]

2.3. Materials Characterization. UV−vis absorption spectra were collected with an Agilent Cary 100. Fluorescence spectra were acquired on an Agilent Eclipse spectrophotometer. AFM measurements were carried out on a Veeco MultiMode V scanning probe microscope in tapping mode. SEM measurement was performed with an FEI Nova Nano 630 (FEI Corporation) with a helix detector in low vacuum (0.43 Torr water pressure). To make samples for either AFM or SEM measurements, the MP-PTCDI nanoribbons were directly transferred from ethanol and deposited onto a silicon substrate coated with a polished 300 nm thick SiO_2 layer, and then dried in vacuum oven at room temperature in the dark.

2.4. Current Measurement. Interdigitated electrodes (IDE) were used for all current measurements in this work. The IDE has a channel width of 2100 μm and a gap length of 50 μm, and was fabricated by a standard photolithography procedure on a silicon wafer with a 300 nm thermal oxide layer (Silicon Quest International). The electrodes were made by sputtering with 20 nm titanium adhesion layer and 50 nm gold layer. MP-PTCDI nanoribbons were deposited onto IDE by drop-casting, followed by drying in vacuum oven at room temperature in the dark. The electrical conductivity was measured under ambient conditions using a two-probe method on a Signatone S-1160 Probe Station combined with an Agilent 4156C Precision Semiconductor Analyzer. To compare the conductivity of different PTCDI nanomaterials, the nanofibers were assembled by injecting a given molar amount of PTCDI (12 nmol dissolved in a minimal volume of $CHCl_3$) into 100 μL ethanol. The nanofibers thus assembled were dispersed well in ethanol, which were then transferred onto the IDE by slow drop-casting to ensure uniform coverage over the whole IDE area. To compare the current enhancement ratio after surface coating with amines, 12 nmol of CH-PTCDI nanobelts were chosen as the standard, zero-doping material, and deposited onto the IDE. One μL of methanol solution containing different concentrations of the amines (1-methylpiperidine, TCI America, > 99.0%; hexylamine, Acros Organics, 99%; triethylamine, Sigma-Aldrich, 99%; aniline, Acros Organics, 99.5%, extra pure) were drop cast onto the surface of the CH-PTCDI nanobelts, providing the varying molar amount of amine coated on the surface. To avoid the oxidation of amines during processing, the fresh amine solution was made for each measurement. ^{1}H NMR measurements were conducted for all the amines during the project period to ensure that the high purity of amines remained throughout the experiments (Supporting Information).

2.5. Chemical Vapor Sensing Measurement. All chemical vapor sensing tests were conducted under ambient conditions in the dark. Figure S2 depicts the sensing and chemical vapor delivery systems. A certain amount of chemical vapor was pulled into a 50 mL syringe and delivered by syringe pump (NE-4000 New Era Pump System, Inc.) at a rate of 25 mL/min into the carrier gas. The carrier gas was dry air with a flow rate of 475 mL/min. The final concentration of chemical vapor in the testing chamber was calculated from the syringe volume and the concentration of original chemical vapor. The original H_2O_2 vapor was generated from 44.7 wt % H_2O_2 solution (Sigma-Aldrich, 50 wt % in H_2O).[30] The IDE chip (deposited with PTCDI nanomaterials) was placed on a ceramic chip carrier

DOI: 10.1021/acsami.6b03151
ACS Appl. Mater. Interfaces 2016, 8, 12360−12368

connected by wire bonding. The ceramic chip carrier was fixed on a breadboard, enclosed in a small Teflon chamber (3.84 cm in length, 1.86 cm in width, and 2.41 cm in height), and connected to an Agilent 4156C Semiconductor Analyzer. A bias of 10 V was applied across the electrodes, and the current through the sensor was monitored. For H_2O_2 testing, the chip was exposed to H_2O_2 vapor for 30 s with a recovery time of 2.5 min. For testing toward the common liquid samples, the exposure time was 30 s with a recovery time of 30 s. The sensing response time of MP-PTCDI nanoribbons was obtained by fitting the time-course current change profile to an exponential function,[31] which gives the response time as 1/e of the time constant obtained.

3. RESULTS AND DISCUSSION

3.1. Synthesis of MP-PTCDI Molecules and Self-Assembly into Nanoribbons. PTCDI-based molecules have been extensively explored for 1D self-assembly and optoelectronic applications in recent years.[20,32−35] Side-chain substitutions do not significantly influence the electronic property of the PTCDI backbone because the two imide positions in the PTCDI molecules are nodes in the π−orbitals.[32,36] This allows for comparative study of the PTCDI materials, for which the side-chain substitutions play an important role in intermolecular interactions, resulting in different electronic properties through charge transfer.[37] In this study, a PTCDI molecule substituted with 1-methylpiperidine moiety (Figure 1, denoted as MP-PTCDI) was designed

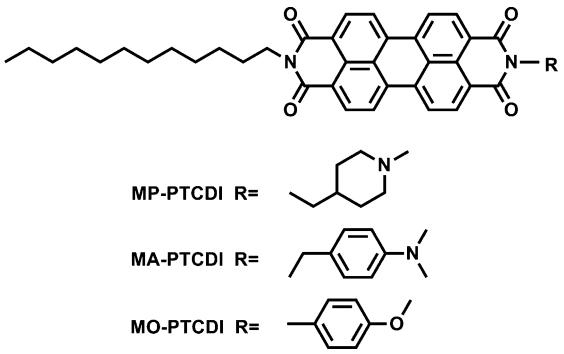

Figure 1. Molecular structures of MP-PTCDI and two other PTCDI analogues, MA-PTCDI and MO-PTCDI, employed for comparative study.

and synthesized. The MP-PTCDI nanoribbons were fabricated using the previously reported solution phase self-assembly method.[20,21,35] The morphology of MP-PTCDI nanoribbons was characterized by SEM and AFM (Figure 2). The nanoribbons are several micrometers in length and 100−300 nm in width. The thickness of the nanoribbons is estimated to be just about 15 nm (Figure 2B−D, AFM images and height-profile). Such shape-defined 1D nanoribbon structures are conducive to the construction of electronic devices. For comparative study, two other PTCDI molecules, MA-PTCDI and MO-PTCDI (both substituted with the same dodecyl alkyl chain but with different groups on the other end, as shown in Figure 1), were also synthesized and assembled into nanoribbon structures following the previously reported methods.[21] Owing to the similar molecular structure, the two reference PTCDIs formed about the same nanoribbon morphology as the MP-PTCDI (see Table S1). The dimethylaniline moiety of MA-PTCDI acts as a strong electron donor under photoexcitation, whereas the methoxyphenyl is not an effective donor to PTCDI as evidenced from our previous investigation.[21] In the next section, we compared the electrical conductivity of the nanoribbons assembled from the three PTCDI building blocks shown in Figure 1, aiming to explore the effects of the side groups on self-doping.

3.2. High Conductivity and Mechanism Study. As shown in Figure 3, MP-PTCDI nanoribbons possess the highest electrical conductivity; the current of the MP-PTCDI nanoribbons is 4 orders of magnitude higher than the other PTCDI nanoribbon materials under the same test conditions. Considering the similar nanoribbon structures formed from the three PTCDIs (Table S1) and the fact that the π−electronic property of PTCDI backbone remains unchanged with different side-substitutions, we concluded that the high conductivity observed for MP-PTCDI nanoribbons is largely caused by the methylpiperidine moiety.[19]

To gain insight into the high conductivity of MP-PTCDI nanoribbons, a case study model was constructed by coating 1-methylpiperidine molecules on *N*,*N*′-di (cyclohexyl)-perylene-3,4,9,10-tetracarboxylic diimide (CH-PTCDI) nanobelts to investigate the influence of this specific substitution group on the conductivity of 1D PTCDI nanomaterials.[38,39] The CH-PTCDI was selected because the cyclohexyl side-chain groups are neutral and inactive in charge transfer interaction, and the shape-defined nanobelts can be easily fabricated from this molecule with high reproducibility.[29] In this study, 12 nmol of CH-PTCDI nanobelts were deposited onto interdigitated electrodes (IDEs) patterned on a silicon wafer, and a controlled amount of 1-methylpiperidine was drop-cast onto the nanobelts (Figure 4A). Negligible currents were measured for either pristine CH-PTCDI nanobelts (0.0012 nA at a bias of 10 V, Figure S3) or pure 1-methylpiperidine film drop-cast from 4 μmol amount (0.0055 nA at a bias of 10 V, Figure S3). In contrast, a much increased current was observed for the CH-PTCDI nanobelts coated with only 2 μmol of 1-methylpiperidine (0.45 nA at a bias of 10 V, Figure S3). The current increased further when more 1-methylpiperidine was deposited. The current increased to 32.5 μA, an enhancement ratio of 2×10^7 compared to the pristine nanobelt, when 4 μmol of 1-methylpiperidine was deposited (Figure 4B). An enhancement ratio of 8×10^6 was observed when 8 μmol of 1-methylpiperidine was deposited, indicating that the current increase started to reach saturation when more than 4 μmol of 1-methylpiperidine was cast (Figure 4B). This significant increase in conductivity is likely due to the chemical doping, which occurs through the donor−acceptor (charge transfer) interaction between 1-methylpiperidine and PTCDI.

The morphology of the CH-PTCDI nanobelts before and after surface coating remained unchanged, as characterized by SEM (Figure 4C,D). Interestingly, the built up surface charging on the pristine CH-PTCDI nanobelts was eliminated by surface coating with 1-methylpiperidine. The SEM image of pristine CH-PTCDI nanobelts shows bright imaging contrast on the surface of the nanobelts, which is a characteristic of the surface charge built up on the nonconductive sample after E-beam exposure during SEM measurement (Figure 4C).[40] However, such surface charging was suppressed after surface coating of the 1-methylpiperidine (Figure 4D). This phenomenon is common in SEM measurements performed on nonconductive samples, for which a thin layer of metal, such as Au, Pt, or Pd, is typically deposited on the sample surface to facilitate charge transmission and prevent charge building up.[40,41] Because the pure 1-methylpiperidine film is slightly conductive (Figure S3), the observed conductivity improvement should be due to the

DOI: 10.1021/acsami.6b03151
ACS Appl. Mater. Interfaces 2016, 8, 12360−12368

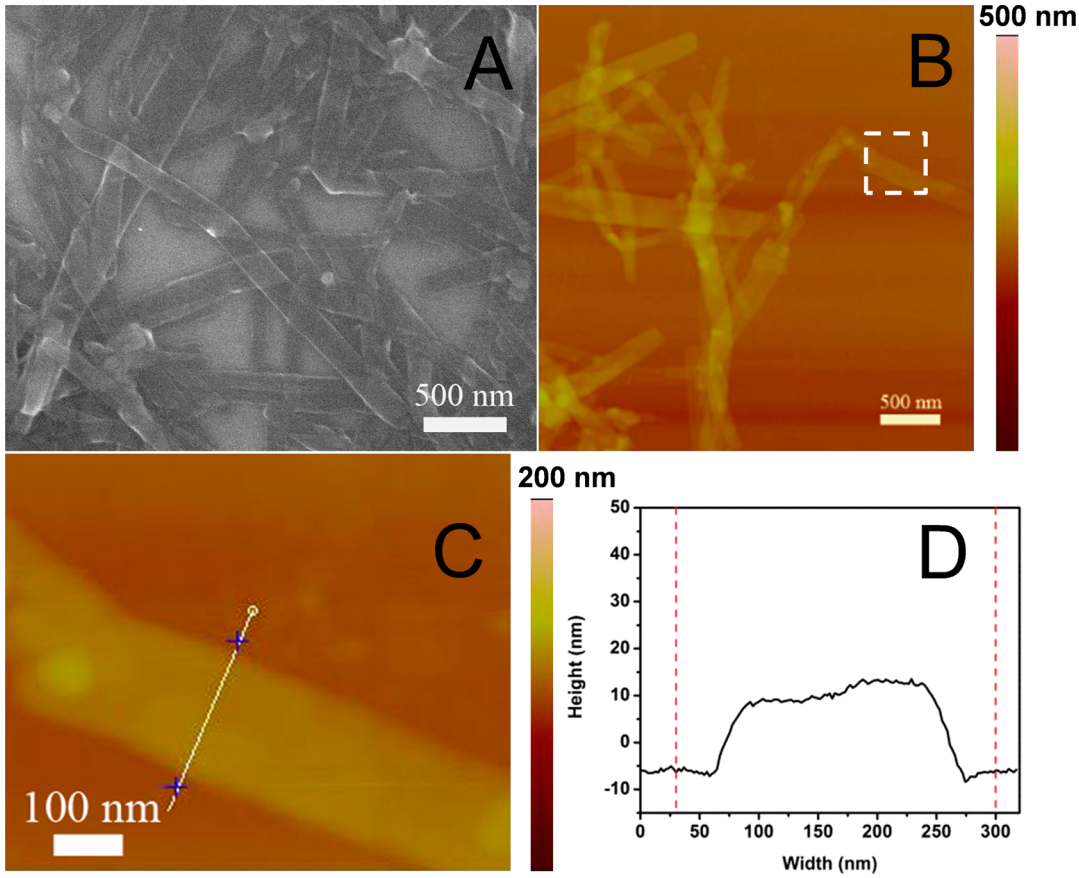

Figure 2. (A) SEM image of MP-PTCDI nanoribbons. (B) AFM image of MP-PTCDI nanoribbons. (C) Enlarged AFM image of the MP-PTCDI nanoribbon in the selected area in panel B. (D) The height-profile corresponding to the white line in panel C.

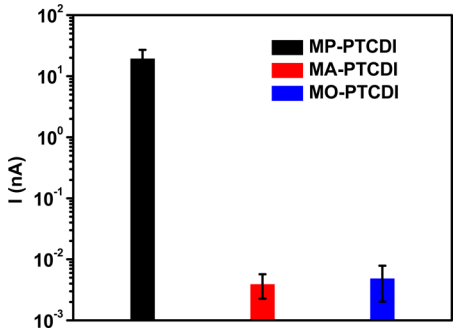

Figure 3. Comparison of the electrical current measured over three PTCDI nanoribbons deposited in the same molar amount (12 nmol), following the same experimental process. The current values were measured at a bias of 10 V. The error bars represent the standard deviation based on the current measured by three independent devices of each PTCDI nanoribbon.

charge transfer interaction between 1-methylpiperidine and CH-PTCDI nanobelts, consistent with the current enhancement discussed above.

The charge transfer interaction between 1-methylpiperidine and CH-PTCDI was also confirmed by the fluorescence quenching measurements of PTCDI. MP-PTCDI solution in chloroform exhibits strong fluorescence emission, comparable to CH-PTCDI molecules in chloroform (Figure S4),[29] indicating that there is no intramolecular electron transfer in the MP-PTCDI molecule. However, no fluorescence emission was observed for the nanoribbons fabricated from the MP-PTCDI molecules (Figure S5A–C). By contrast, the CH-PTCDI nanobelts still have considerable fluorescence emission (Figure S5D–F). The fluorescence quenching within MP-PTCDI nanoribbons is likely caused by the intermolecular electron transfer between 1-methylpiperidine on one molecule and the PTCDI part on the other molecule. To prove this intermolecular charge transfer, fluorescence spectra of the reference PTCDI, CH-PTCDI, were measured in chloroform solutions with and without the addition of 1-methylpiperidine (Figure S6A). Significant fluorescence quenching (indicative of charge transfer interaction) was observed with increasing the concentration of 1-methylpiperidine, which follows the linear Stern–Volmer relationship (Figure S6B). The linear fitting gives the binding constant of 21.6 M^{-1} between 1-methylpiperidine and the PTCDI. The binding constant obtained is about 1 order of magnitude higher than those measured for the aromatic hydrocarbon donor–acceptor complexes reported by others.[42] The enhanced binding is largely due to the stronger electron donating capability of organic amines, compared to the aromatic hydrocarbons.

To determine whether other amines can interact with PTCDI as strong as 1-methylpiperidine, we selected aniline, hexylamine, and triethylamine for comparative testing. Following the same experimental procedure of surface doping as described above, different amount of amines were drop-cast onto the surface of the CH-PTCDI nanobelts. As shown in Figure S7A, when 0.5 μmol of amine was applied, no obvious current enhancement was obtained by coating with aniline, hexylamine, and triethylamine, whereas a 26-fold increase in

DOI: 10.1021/acsami.6b03151
ACS Appl. Mater. Interfaces 2016, 8, 12360–12368

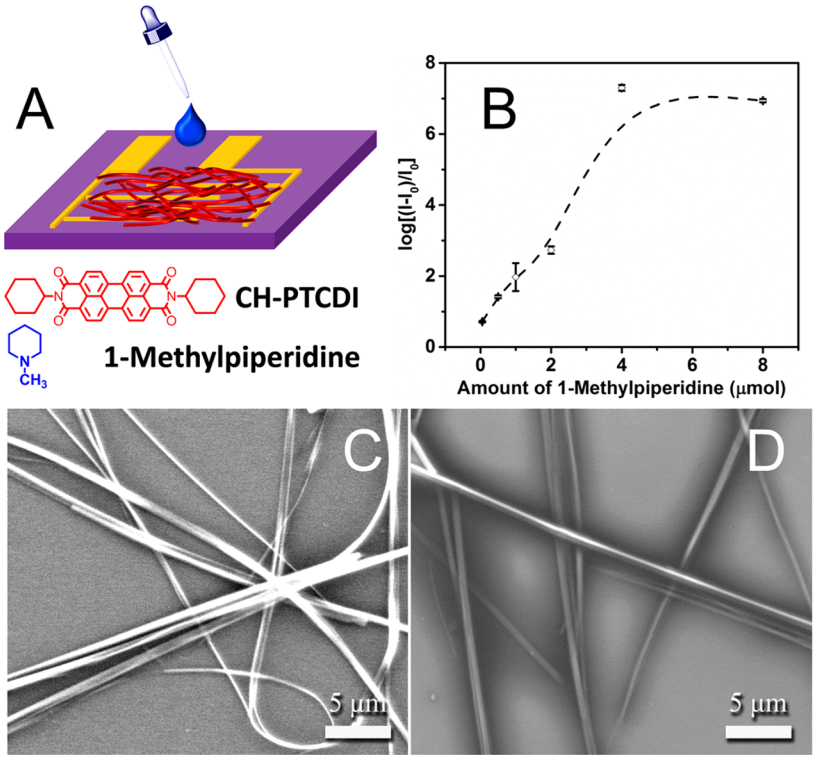

Figure 4. (A) Schematic of the CH-PTCDI nanobelts deposited on the IDE and the surface coating by drop-casting the solution of 1-methylpiperidine. (B) The current enhancement ratio, $\log[(I - I_0)/I_0]$, measured over the CH-PTCDI nanobelts when coated with varying molar amounts of 1-methylpiperidine, where I_0 is the current of pristine CH-PTCDI nanobelts, and I is the current measured on the same nanobelts after coated with 1-methylpiperidine. The error bars stand for the standard deviation based on the values measured by three independent devices. All the current values were obtained at a bias of 10 V. (C, D) SEM images of the CH-PTCDI nanobelts before (C) and after (D) surface coating with 1-methylpiperidine.

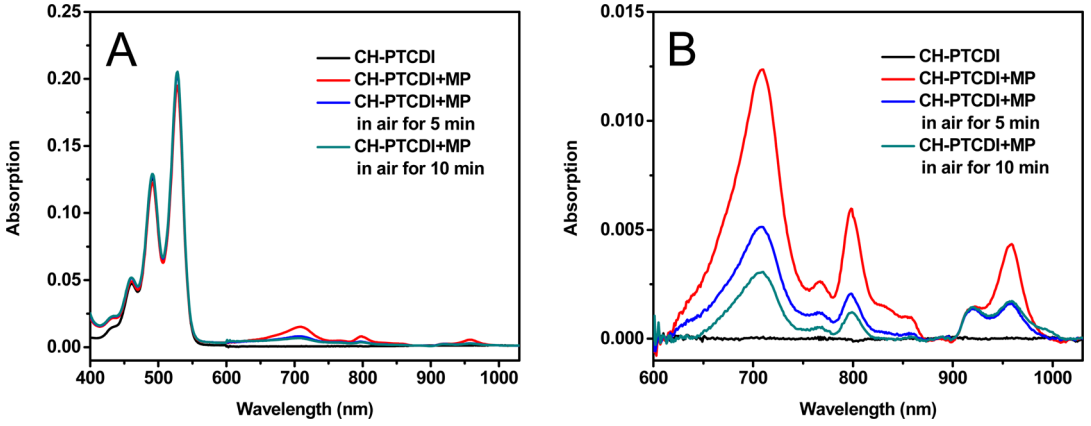

Figure 5. (A) UV−vis absorption spectra of deoxygenated DMSO solution of CH-PTCDI (10 μmol/L) before (black) and after (red) addition of excessive 1-methylpiperidine (MP, 0.1 mol/L), and the same solution after exposed to air for 5 min (blue) and 10 min (dark cyan). (B) Enlarged UV−vis absorption spectra of (A) in the wavelength range of 600 to 1000 nm.

current was observed by coating with 1-methylpiperidine under the same condition. However, significant increase in current was observed when the amount of hexylamine and triethylamine increased to 8 μmol, for which the enhancement ratios were about 3000 and 1800, respectively (though still 3 orders of magnitude lower than 1-methylpiperidine), whereas aniline still produced negligible current even with as much as 12 μmol coated (Figure S7B).

Regarding the fact that the CH-PTCDI nanobelts coated by the three amines under study (1-methylpiperidine, hexylamine, and triethylamine) produced enhanced conductivity relative to the pristine CH-PTCDI nanobelts while those treated with aniline did not, we further studied the interaction between CH-PTCDI molecules and amines using UV−vis absorption spectroscopy. Inspired by our previous work,[16] in which a strong electron donor (e.g., hydrazine) reduced PTCDI molecules to anionic radicals, we also detected the PTCDI anionic radical upon adding the three amines into the oxygen free solution of CH-PTCDI in dimethyl sulfoxide (DMSO). The existence of three new absorption peaks at 708, 798, and 959 nm in the presence of 1-methylpiperidine indicates the formation of PTCDI anionic radicals (Figure 5).[16,17,43] In the

DOI: 10.1021/acsami.6b03151
ACS Appl. Mater. Interfaces 2016, 8, 12360−12368

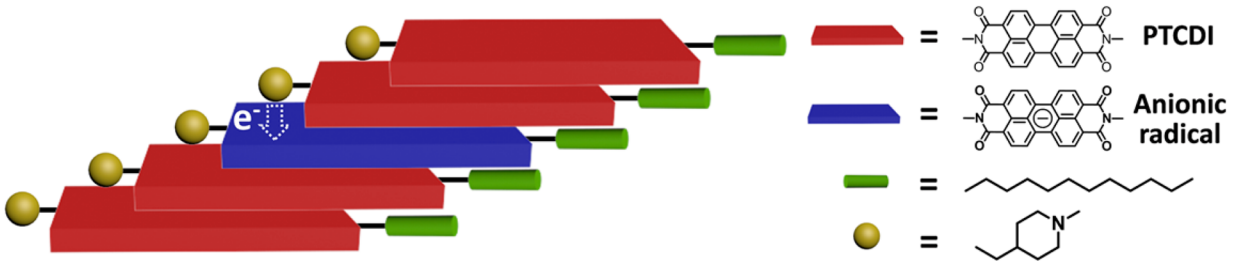

Figure 6. Schematic of the conductivity enhancement of MP-PTCDI nanoribbons.

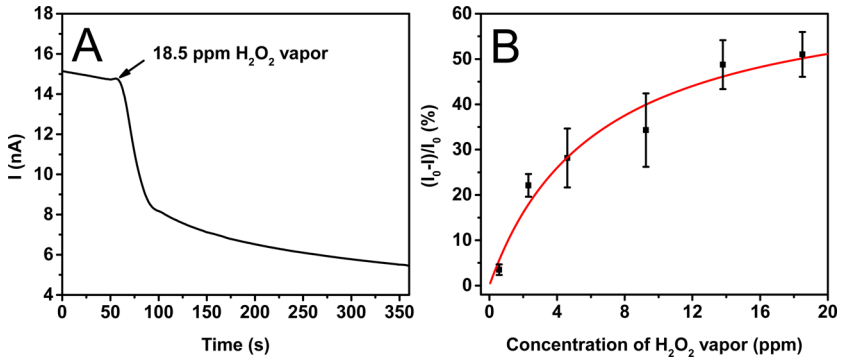

Figure 7. (A) Current measured over the MP-PTCDI nanoribbons in response to H_2O_2 vapor (18.5 ppm). (B) Relative current change $[(I_0 - I)/I_0$ (%)] as a function of the concentration of H_2O_2 vapor, where I and I_0 are the current measured before and after exposure to H_2O_2 vapor, respectively. The error bars represent the standard deviation of the relative current changes measured with three independent sensors under each concentration. Details of how to define I and I_0 and to calculate $(I_0 - I)/I_0$ can be found in Figure S9. The data are fitted with Langmuir adsorption model (Supporting Information).

absence of oxygen, the radicals are very stable. Upon exposure to air, the three characteristic peaks diminish with time, which further confirms the formation of oxygen-sensitive PTCDI anionic radicals. Moreover, analysis based on the redox potentials suggests that the electron transfer from 1-methylpiperidine to PTCDI is a thermodynamic favorable (spontaneous) process (Supporting Information). In addition to 1-methylpiperidine, PTCDI anionic radicals were also generated by addition of hexylamine and triethylamine (Figure S8). However, no such anionic radicals were generated upon addition of aniline to the same deoxygenated solution of CH-PTCDI (Figure S8). This comparative observation is consistent with the above-discussed results of conductivity enhancement upon casting of different amines, indicating that the effective charge transfer interaction (thus generating PTCDI anionic radical) is the primary cause of the conductivity enhancement. The electrons thus generated can delocalize (migrate) along the $\pi-\pi$ stacking of PTCDIs,[20,34,44] acting as the major charge carrier for the n-type material.

The electron donating strength of amines can be evaluated by the oxidation potentials as others did for evaluating the charge transfer in different donor–acceptor pairs.[42] Among all the amines used in this project, aniline would be the strongest electron donor from their oxidation potentials (1-methylpiperidine, E^{o}_{ox} = 1.08 V vs SCE;[45] hexylamine, E^{o}_{ox} = 1.44 V vs SCE;[46] triethylamine, E^{o}_{ox} = 0.99 V vs SCE;[47] aniline, E^{o}_{ox} = 0.86 V vs SCE[47]). However, as evidenced by our results, no charge transfer was observed between aniline and PTCDI even in the presence of a large excess of aniline (i.e., no significant current enhancement was observed with 12 μmol aniline coated on the CH-PTCDI nanobelts, and no absorption peaks of PTCDI anionic radical were detected in the deoxygenated DMSO solution of CH-PTCDI (10 μmol/L) in the presence of excessive aniline (0.1 mol/L)). The lack of charge transfer between aniline and PTCDI might be due to the weak nucleophilicity of aniline,[48] which prevents the strong donor–acceptor interaction.

On the basis of the aforementioned results and discussion, we propose a possible n-type doping mechanism, which is a result of the generation of PTCDI anionic radicals, to explain the high conductivity of the MP-PTCDI nanoribbons. As demonstrated in Figure 6, upon self-assembly into nanoribbons, the side groups of 1-methylpiperidine are in close proximity of the PTCDI backbones, enabling charge transfer interaction to form PTCDI anionic radicals (the reduction of PTCDI by 1-methylpiperidine should be more thermodynamically favored in solid state compared to solution phase due to the much higher local concentration in solid; Supporting Information). Owing to the efficient intramolecular π–electron delocalization within the PTCDI plane, the electron (anionic radical) generated can be well stabilized (against charge recombination) as observed in the UV–vis absorption spectral measurement (Figure 5). When this occurs inside the nanoribbons, the electron can effectively survive from the scavenging by oxygen, making the high conductivity gained sustainable even in the ambient environment as indeed observed in this study (Figures 3 and 4). With an applied bias, the self-doped electrons rapidly migrate along the long axis of the nanoribbon facilitated by the intermolecular $\pi-\pi$ electron delocalization,[16,44,49] leading to the high conductivity. The resultant PTCDI anionic radical is an n-type dopant and is similar to the ones employed in other works,[13−15] in which the substitutional dopant was a zwitterionic molecule, a PTCDI anionic radical linked to an amine centered cation (a reduced analogue of the PTCDI host molecule). An n-doped PTCDI film was fabricated by spin-coating mixed PTCDI dopant and host materials solution,

DOI: 10.1021/acsami.6b03151
ACS Appl. Mater. Interfaces 2016, 8, 12360−12368

resulting in 10 orders of magnitude of increase in conductivity with just 1% doping. The doping process reported in this work is also similar to the self-doped conductor of tetrathiafulvalene (TTF) derivative.[50] TTFCOOH is an insulator, but upon reaction with NH_3, it switches into a conductor $TTFCOO^-NH_4^+$ with a conductivity of 2×10^{-4} S/cm. It was demonstrated that the conductivity gained in the salt came from a radical species $TTF^{\bullet+}COO^-NH_4^+$ generated by self-protonation of the TTF moiety.

3.3. Chemiresistive Sensing for Hydrogen Peroxide Vapor Detection. With the increased electrical conductivity by self-doping, MP-PTCDI nanoribbons can be a potential building material for chemiresistive sensors, for which the high conductivity improves the signal-to-noise ratio and simplifies the system design. A chemiresistive sensor based on the nanoribbons benefits from the large surface area and continuous porosity formed by the interlaced nanoribbons deposited on the substrate. Combining these two features enhances the adsorption and diffusion (accumulation) of gas analytes, thus increasing the sensitivity to the analytes. The n-type character of the PTCDI material allows for chemiresistive sensing of electron deficient analytes, which can be bound to the surface, causing charge depletion of the material. In this study, we chose H_2O_2 vapor as the target analyte because it is a critical signature for the peroxide explosives including both the synthetic ones (e.g., TATP, DADP, and HMTD) and the simple liquid mixtures of H_2O_2 and the fuels.[22]

Figure 7A shows the real-time electrical current profile of a MP-PTCDI nanoribbon chemiresistor sensor in response to H_2O_2 vapor. Upon exposure to H_2O_2 vapor (18.5 ppm), there is an instantaneous decrease in current of about 50%. A very short response time of 19.5 s is attributed to the large surface area of nanoribbons and expedient diffusion of H_2O_2 vapor. The response is concentration dependent. Figure 7B shows a plot of relative sensor response as a function of the concentration of H_2O_2 vapor, which can fit well into the Langmuir absorption model (Supporting Information).[5] The lowest concentration of H_2O_2 vapor tested in this study was 0.6 ppm, which represents the lowest level that can be provided by the present experimental setup.[51] This level of H_2O_2 vapor represents 2 orders of magnitude dilution of the saturated vapor of commercial 50 wt % H_2O_2 solution. The irreversible sensor response toward H_2O_2 is attributed to the strong surface binding of H_2O_2 and the permanent oxidation of 1-methylpiperidine groups by H_2O_2 (E^o_{red} = 1.78 V, vs SCE).[52]

In addition to the high sensitivity, the MP-PTCDI nanoribbons also demonstrated high selectivity toward H_2O_2 vapor against water and the common organic liquids, facilitating the development into practical sensing applications. Such general selectivity was investigated by measuring the sensor response toward the vapor of various common liquids, including water, acetone, ethyl acetate, dichloromethane, methanol, ethanol, toluene, and hexane. In contrast to the irreversible decrease response caused by H_2O_2 vapor, exposure to these liquids vapor resulted in reversible increase in current for the MP-PTCDI nanoribbons (Figure S10). The increased conductivity observed is likely a result of dipole interaction between MP-PTCDI nanoribbon and the liquid molecule.[53,54] Table S2 lists the dipole moments of all the liquid analytes tested and the corresponding sensor responses measured at 5% of the saturated vapor concentration. Clearly, the sensing response and the dipole moment of the liquids are tightly correlated. For liquids with smaller dipole moments, the response is lower. For example, the vapor concentration of hexane used (8400 ppm) is much higher than many other analytes, such as ethyl acetate (4900 ppm), water (1100 ppm), ethanol (3000 ppm), toluene (1500 ppm), but the relative response is only 0.1%, the lowest among all chemicals studied here, because the dipole moment of hexane is less than 0.1 D, much lower than others.

4. CONCLUSIONS

In conclusion, the nanoribbons assembled from the 1-methylpiperidine substituted-PTCDI molecules possess extraordinarily high conductivity relative to other PTCDI-based nanostructures. The 1-methylpiperidine group plays a key role in the conductivity enhancement, as evidenced by systematic experiments and analysis of the interaction between a model PTCDI nanobelt and 1-methylpiperidine. Upon self-assembly into one-dimensional nanoribbons, the 1-methylpiperidine groups interact with the PTCDI core in stacking proximity to produce the PTCDI anionic radical, which acts as the n-type dopant in the PTCDI lattice. The doping process increases the charge carrier density within the PTCDI nanoribbons (Supporting Information), and the 1D $\pi-\pi$ stacking of PTCDIs is efficient for long-range charge migration, thereby resulting in high conductivity. The high conductivity obtained enables application in chemiresistive sensors. The PTCDI nanoribbons demonstrated highly sensitive response to H_2O_2 vapor through oxidation, rather than dipole moment interaction as in the case of common liquid vapor, thereby producing general selectivity toward H_2O_2 vapor. Owing to the high conductivity of MP-PTCDI nanoribbons, as well as the porous mesh-like morphology of the nanoribbon film, the lowest detected concentration of H_2O_2 vapor in this study was down to 0.6 ppm. This work provides an alternative approach to fabricating self-doped organic semiconductors with high conductivity by molecular engineering.

■ ASSOCIATED CONTENT

Supporting Information

The Supporting Information is available free of charge on the ACS Publications website at DOI: 10.1021/acsami.6b03151.

Chemical structure and synthesis method of Compound 1, schematic diagram of the vapor sensing measurement system, table comparing morphology and size of PTCDI-based nanostructures, $I-V$ curves of pure 1-methylpiperidine film, CH-PTCDI nanobelts before and after surface coating with 1-methylpiperidine, UV−vis absorption and fluorescence spectra and images, calculation of the Gibbs free energy change of the electron transfer between 1-methylpiperidine and CH-PTCDI molecules, a plot demonstrating how to calculate the current decrease of MP-PTCDI nanoribbons in response to H_2O_2 vapor, data fitting with the Langmuir absorption model, sensor response toward common solvents, the dipole moment of common liquid tested, an interpretation of enhanced conductivity due to increase in charger carrier density, and ^1H NMR of amines. (PDF)

■ AUTHOR INFORMATION

Corresponding Author

* E-mail: lzang@eng.utah.edu.

DOI: 10.1021/acsami.6b03151
ACS Appl. Mater. Interfaces 2016, 8, 12360−12368

Author Contributions

The manuscript was written through contributions of all authors. All authors have given approval to the final version of the manuscript.

Notes

The authors declare no competing financial interest.

■ ACKNOWLEDGMENTS

This work was supported by the Department of Homeland Security, Science and Technology Directorate under Grant (2009-ST-108-LR0005), NSF (CHE 0931466), NSF (CBET 1502433), the SEED grant of the VP office of University of Utah (award # 10029849), and USTAR program. B. R. B. acknowledges support from the NASA Office of the Chief Technologist (NNX12AM67H) and the National Science Foundation IGERT (DGE0903715).

■ REFERENCES

(1) Allard, S.; Forster, M.; Souharce, B.; Thiem, H.; Scherf, U. Organic Semiconductors for Solution-Processable Field-Effect Transistors(OFETs). *Angew. Chem., Int. Ed.* **2008**, *47*, 4070−4098.

(2) Gross, M.; Muller, D. C.; Nothofer, H.-G.; Scherf, U.; Neher, D.; Brauchle, C.; Meerholz, K. Improving the Performance of Doped π-Conjugated Polymers for Use in Organic Light-Emitting Diodes. *Nature* **2000**, *405*, 661−665.

(3) Hains, A. W.; Liang, Z.; Woodhouse, M. A.; Gregg, B. A. Molecular Semiconductors in Organic Photovoltaic Cells. *Chem. Rev.* **2010**, *110*, 6689−6735.

(4) Baeg, K.-J.; Binda, M.; Natali, D.; Caironi, M.; Noh, Y.-Y. Organic Light Detectors: Photodiodes and Phototransistors. *Adv. Mater.* **2013**, *25*, 4267−4295.

(5) Huang, H.; Gross, D. E.; Yang, X.; Moore, J. S.; Zang, L. One-Step Surface Doping of Organic Nanofibers to Achieve High Dark Conductivity and Chemiresistor Sensing of Amines. *ACS Appl. Mater. Interfaces* **2013**, *5*, 7704−7708.

(6) Medina-Sánchez, M.; Martínez-Domingo, C.; Ramon, E.; Merkoçi, A. An Inkjet-Printed Field-Effect Transistor for Label-Free Biosensing. *Adv. Funct. Mater.* **2014**, *24*, 6291−6302.

(7) Chan, C. K.; Kim, E. G.; Brédas, J. L.; Kahn, A. Molecular n-Type Doping of 1,4,5,8-Naphthalene Tetracarboxylic Dianhydride by Pyronin B Studied Using Direct and Inverse Photoelectron Spectroscopies. *Adv. Funct. Mater.* **2006**, *16*, 831−837.

(8) Walzer, K.; Maennig, B.; Pfeiffer, M.; Leo, K. Highly Efficient Organic Devices Based on Electrically Doped Transport Layers. *Chem. Rev.* **2007**, *107*, 1233−1271.

(9) Lu, C.-K.; Meng, H.-F. Hole Doping by Molecular Oxygen in Organic Semiconductors: Band-Structure Calculations. *Phys. Rev. B: Condens. Matter Mater. Phys.* **2007**, *75*, 235206.

(10) Yamamoto, Y.; Yoshino, K.; Inuishi, Y. Electrical Properties of Phthalocyanine-Halogen Complexes. *J. Phys. Soc. Jpn.* **1979**, *47*, 1887−1891.

(11) Maennig, B.; Pfeiffer, M.; Nollau, A.; Zhou, X.; Leo, K.; Simon, P. Controlled p-Type Doping of Polycrystalline and Amorphous Organic Layers: Self-Consistent Description of Conductivity and Field-Effect Mobility by a Microscopic Percolation Model. *Phys. Rev. B: Condens. Matter Mater. Phys.* **2001**, *64*, 195208.

(12) Werner, A. G.; Li, F.; Harada, K.; Pfeiffer, M.; Fritz, T.; Leo, K. Pyronin B as a Donor for n-Type Doping of Organic Thin Films. *Appl. Phys. Lett.* **2003**, *82*, 4495−4497.

(13) Gregg, B. A.; Cormier, R. A. Doping Molecular Semiconductors: n-Type Doping of a Liquid Crystal Perylene Diimide. *J. Am. Chem. Soc.* **2001**, *123*, 7959−7960.

(14) Chen, S.-G.; Branz, H. M.; Eaton, S. S.; Taylor, P. C.; Cormier, R. A.; Gregg, B. A. Substitutional n-Type Doping of an Organic Semiconductor Investigated by Electron Paramagnetic Resonance Spectroscopy. *J. Phys. Chem. B* **2004**, *108*, 17329−17336.

(15) Gregg, B. A.; Chen, S.-G.; Cormier, R. A. Coulomb Forces and Doping in Organic Semiconductors. *Chem. Mater.* **2004**, *16*, 4586−4599.

(16) Che, Y.; Datar, A.; Yang, X.; Naddo, T.; Zhao, J.; Zang, L. Enhancing One-Dimensional Charge Transport through Intermolecular π-Electron Delocalization: Conductivity Improvement for Organic Nanobelts. *J. Am. Chem. Soc.* **2007**, *129*, 6354−6355.

(17) Arulkashmir, A.; Jain, B.; John, J. C.; Roy, K.; Krishnamoorthy, K. Chemically Doped Perylene Diimide Lamellae Based Field Effect Transistor with Low Operating Voltage and High Charge Carrier Mobility. *Chem. Commun.* **2014**, *50*, 326−328.

(18) Malinauskas, A. Self-Doped Polyanilines. *J. Power Sources* **2004**, *126*, 214−220.

(19) Yue, J.; Epstein, A. J. Synthesis of Self-Doped Conducting Polyaniline. *J. Am. Chem. Soc.* **1990**, *112*, 2800−2801.

(20) Zang, L.; Che, Y.; Moore, J. S. One-Dimensional Self-Assembly of Planar π-Conjugated Molecules: Adaptable Building Blocks for Organic Nanodevices. *Acc. Chem. Res.* **2008**, *41*, 1596−1608.

(21) Che, Y.; Yang, X.; Liu, G.; Yu, C.; Ji, H.; Zuo, J.; Zhao, J.; Zang, L. Ultrathin n-Type Organic Nanoribbons with High Photoconductivity and Application in Optoelectronic Vapor Sensing of Explosives. *J. Am. Chem. Soc.* **2010**, *132*, 5743−5750.

(22) Xu, M.; Han, J.-M.; Wang, C.; Yang, X.; Pei, J.; Zang, L. Fluorescence Ratiometric Sensor for Trace Vapor Detection of Hydrogen Peroxide. *ACS Appl. Mater. Interfaces* **2014**, *6*, 8708−8714.

(23) Xu, M.; Han, J.-M.; Zhang, Y.; Yang, X.; Zang, L. A Selective Fluorescence Turn-On Sensor for Trace Vapor Detection of Hydrogen Peroxide. *Chem. Commun.* **2013**, *49*, 11779−11781.

(24) Abo, M.; Urano, Y.; Hanaoka, K.; Terai, T.; Komatsu, T.; Nagano, T. Development of a Highly Sensitive Fluorescence Probe for Hydrogen Peroxide. *J. Am. Chem. Soc.* **2011**, *133*, 10629−10637.

(25) Xu, M.; Bunes, B. R.; Zang, L. Paper-Based Vapor Detection of Hydrogen Peroxide: Colorimetric Sensing with Tunable Interface. *ACS Appl. Mater. Interfaces* **2011**, *3*, 642−647.

(26) Bai, J.; Jiang, X. A Facile One-Pot Synthesis of Copper Sulfide-Decorated Reduced Graphene Oxide Composites for Enhanced Detecting of H_2O_2 in Biological Environments. *Anal. Chem.* **2013**, *85*, 8095−8101.

(27) Guo, P.; Zhao, G.; Chen, P.; Lei, B.; Jiang, L.; Zhang, H.; Hu, W.; Liu, M. Porphyrin Nanoassemblies Via Surfactant-Assisted Assembly and Single Nanofiber Nanoelectronic Sensors for High-Performance H_2O_2 Vapor Sensing. *ACS Nano* **2014**, *8*, 3402−3411.

(28) Bohrer, F. I.; Colesniuc, C. N.; Park, J.; Schuller, I. K.; Kummel, A. C.; Trogler, W. C. Selective Detection of Vapor Phase Hydrogen Peroxide with Phthalocyanine Chemiresistors. *J. Am. Chem. Soc.* **2008**, *130*, 3712−3713.

(29) Che, Y.; Yang, X.; Balakrishnan, K.; Zuo, J.; Zang, L. Highly Polarized and Self-Waveguided Emission from Single-Crystalline Organic Nanobelts. *Chem. Mater.* **2009**, *21*, 2930−2934.

(30) Manatt, S. L.; Manatt, M. R. R. On the Analyses of Mixture Vapor Pressure Data: The Hydrogen Peroxide/Water System and Its Excess Thermodynamic Functions. *Chem. - Eur. J.* **2006**, *12*, 3695−3695.

(31) Wang, D.; Chen, A.; Jang, S.-H.; Davies, J.; Jen, A. K. Y. The Effect of Dipole Moment and Electron Deficiency of Analytes on the Chemiresistive Response of TiO_2(B) Nanowires. *Analyst* **2011**, *136*, 4179−4182.

(32) Wurthner, F. Perylene Bisimide Dyes as Versatile Building Blocks for Functional Supramolecular Architectures. *Chem. Commun.* **2004**, 1564−1579.

(33) Görl, D.; Zhang, X.; Würthner, F. Molecular Assemblies of Perylene Bisimide Dyes in Water. *Angew. Chem., Int. Ed.* **2012**, *51*, 6328−6348.

(34) Zang, L. Interfacial Donor−Acceptor Engineering of Nanofiber Materials to Achieve Photoconductivity and Applications. *Acc. Chem. Res.* **2015**, *48*, 2705−2714.

(35) Chen, S.; Slattum, P.; Wang, C.; Zang, L. Self-Assembly of Perylene Imide Molecules into 1d Nanostructures: Methods, Morphologies, and Applications. *Chem. Rev.* **2015**, *115*, 11967−11998.

DOI: 10.1021/acsami.6b03151
ACS Appl. Mater. Interfaces 2016, 8, 12360−12368

(36) Kazmaier, P. M.; Hoffmann, R. A Theoretical Study of Crystallochromy. Quantum Interference Effects in the Spectra of Perylene Pigments. *J. Am. Chem. Soc.* **1994**, *116*, 9684−9691.
(37) Lei, T.; Luo, J.; Wang, L.; Ma, Y.; Wang, J.; Cao, Y.; Pei, J. Highly Stable Blue Light-Emitting Materials with a Three-Dimensional Architecture: Improvement of Charge Injection and Electroluminescence Performance. *New J. Chem.* **2010**, *34*, 699−707.
(38) Che, Y.; Huang, H.; Xu, M.; Zhang, C.; Bunes, B. R.; Yang, X.; Zang, L. Interfacial Engineering of Organic Nanofibril Heterojunctions into Highly Photoconductive Materials. *J. Am. Chem. Soc.* **2011**, *133*, 1087−1091.
(39) Huang, H.; Chou, C.-E.; Che, Y.; Li, L.; Wang, C.; Yang, X.; Peng, Z.; Zang, L. Morphology Control of Nanofibril Donor−Acceptor Heterojunction to Achieve High Photoconductivity: Exploration of New Molecular Design Rule. *J. Am. Chem. Soc.* **2013**, *135*, 16490−16496.
(40) Cazaux, J. About the Mechanisms of Charging in EPMA, SEM, and ESEM with Their Time Evolution. *Microsc. Microanal.* **2004**, *10*, 670−684.
(41) Moncrieff, D. A.; Robinson, V. N. E.; Harris, L. B. Charge Neutralisation of Insulating Surfaces in the Sem by Gas Ionisation. *J. Phys. D: Appl. Phys.* **1978**, *11*, 2315.
(42) Rathore, R.; Lindeman, S. V.; Kochi, J. K. Charge-Transfer Probes for Molecular Recognition Via Steric Hindrance in Donor-Acceptor Pairs. *J. Am. Chem. Soc.* **1997**, *119*, 9393−9404.
(43) Ghosh, I.; Ghosh, T.; Bardagi, J. I.; König, B. Reduction of Aryl Halides by Consecutive Visible Light-Induced Electron Transfer Processes. *Science* **2014**, *346*, 725−728.
(44) Coropceanu, V.; Cornil, J.; da Silva Filho, D. A.; Olivier, Y.; Silbey, R.; Brédas, J.-L. Charge Transport in Organic Semiconductors. *Chem. Rev.* **2007**, *107*, 926−952.
(45) Jakubiak, J.; Allonas, X.; Fouassier, J. P.; Sionkowska, A.; Andrzejewska, E.; Linden, L. Å.; Rabek, J. F. Camphorquinone−Amines Photoinitating Systems for the Initiation of Free Radical Polymerization. *Polymer* **2003**, *44*, 5219−5226.
(46) Barnes, K. K.; Mann, C. K. Electrochemical Oxidation of Primary Aliphatic Amines. *J. Org. Chem.* **1967**, *32*, 1474−1479.
(47) Reppy, M. A.; Cooper, M. E.; Smithers, J. L.; Gin, D. L. A Novel Fluorescent Monomer for the Selective Detection of Phenols and Anilines. *J. Org. Chem.* **1999**, *64*, 4191−4195.
(48) Bunnett, J. F.; Davis, G. T. The Nucleophilic Reactivity of Aniline, Hydrazine and Phenoxide Ion toward 2,4-Dinitrochlorobenzene1. *J. Am. Chem. Soc.* **1958**, *80*, 4337−4339.
(49) Supur, M.; Fukuzumi, S. Energy and Electron Transfer of One-Dimensional Nanomaterials of Perylenediimides. *ECS J. Solid State Sci. Technol.* **2013**, *2*, M3051−M3062.
(50) Kobayashi, Y.; Yoshioka, M.; Saigo, K.; Hashizume, D.; Ogura, T. Hydrogen-Bonding-Assisted Self-Doping in Tetrathiafulvalene-(TTF) Conductor. *J. Am. Chem. Soc.* **2009**, *131*, 9995−10002.
(51) Li, J.; Lu, Y.; Ye, Q.; Cinke, M.; Han, J.; Meyyappan, M. Carbon Nanotube Sensors for Gas and Organic Vapor Detection. *Nano Lett.* **2003**, *3*, 929−933.
(52) Islam, A.-z. N.; Tofik, N. I.; Murtuza, N. T. Coherent-Synchronized Oxidation of 4-Ethylpyridine and Piperidine by Hydrogen Peroxide. *J. Chem. Chem. Eng.* **2013**, *7*, 76−80.
(53) Carsten, B.; Szarko, J. M.; Son, H. J.; Wang, W.; Lu, L.; He, F.; Rolczynski, B. S.; Lou, S. J.; Chen, L. X.; Yu, L. Examining the Effect of the Dipole Moment on Charge Separation in Donor−Acceptor Polymers for Organic Photovoltaic Applications. *J. Am. Chem. Soc.* **2011**, *133*, 20468−20475.
(54) Wang, B.; Haick, H. Effect of Functional Groups on the Sensing Properties of Silicon Nanowires toward Volatile Compounds. *ACS Appl. Mater. Interfaces* **2013**, *5*, 2289−2299.

DOI: 10.1021/acsami.6b03151
ACS Appl. Mater. Interfaces 2016, 8, 12360−12368